ImpMIA: Leveraging Implicit Bias for Membership Inference Attack under Realistic Scenarios

Anonymous authors
Paper under double-blind review

ABSTRACT

Determining which data samples were used to train a model—known as Membership Inference Attack (MIA)—is a well-studied and important problem with implications for data privacy. Black-box methods presume access only to the model's outputs and often rely on training auxiliary reference models. While they have shown strong empirical performance, they rely on assumptions that rarely hold in real-world settings: (i) the attacker knows the training hyperparameters; (ii) all available non-training samples come from the same distribution as the training data; and (iii) the fraction of training data in the evaluation set is known. In this paper, we demonstrate that removing these assumptions leads to a significant drop in the performance of black-box attacks. We introduce ***ImpMIA***, a Membership Inference Attack that exploits the ***Implicit Bias*** of neural networks, hence removes the need to rely on any reference models and their assumptions. *ImpMIA* is a white-box attack – a setting which assumes access to model weights and is becoming increasingly realistic given that many models are publicly available (e.g., via Hugging Face). Building on maximum-margin implicit bias theory, *ImpMIA* uses the Karush–Kuhn–Tucker (KKT) optimality conditions to identify training samples. This is done by finding the samples whose gradients most strongly reconstruct the trained model's parameters. As a result, *ImpMIA* achieves state-of-the-art performance compared to both black and white box attacks in realistic settings where only the model weights and a superset of the training data are available.

1 INTRODUCTION

Ensuring that trained models do not leak information about their training sets is a critical challenge. Membership inference attacks (MIAs) evaluate this risk by determining whether a given example was part of a model's training data. MIAs can be broadly divided into two categories: black-box, which assume only query access to model outputs (Shokri et al., 2017; Yeom et al., 2018; Li & Zhang, 2021; Carlini et al., 2022), and white-box, which exploit access to internal parameters such as weights or gradients (Nasr et al., 2019; Leino & Fredrikson, 2020; Cohen & Giryes, 2024).

The most effective black-box MIAs are reference-model–based attacks. These methods estimate the distribution of losses for members (training samples) versus non-members by training auxiliary reference models that mimic the target model, thereby learning its loss behavior. However, training large sets of reference models is computationally expensive, and—more importantly—their effectiveness depends on the reference models being accurate surrogates of the target. As a result, these attacks rely on several strong assumptions: (i) the attacker knows the training hyperparameters (e.g., learning rate, optimizer, number of epochs); (ii) the non-training samples come from the same distribution as the training data; and (iii) the fraction of training members in the evaluation set is known. When any of these assumptions is violated, the performance of black-box MIAs drops significantly (Shokri et al., 2017; Salem et al., 2019; Song & Mittal, 2021; Carlini et al., 2022), limiting their reliability for auditing privacy in realistic settings.

On the other hand, white-box MIAs assume access to model weights or gradients. While this is still an assumption, this scenario is increasingly realistic, as many modern models are released with their full parameters publicly available (e.g., via platforms such as Hugging Face). White-box MIAs have shown strong performance by leveraging gradients and activations (Nasr et al., 2019; Leino & Fredrikson, 2020), or influence scores (Cohen & Giryes, 2024). However, despite these advances,
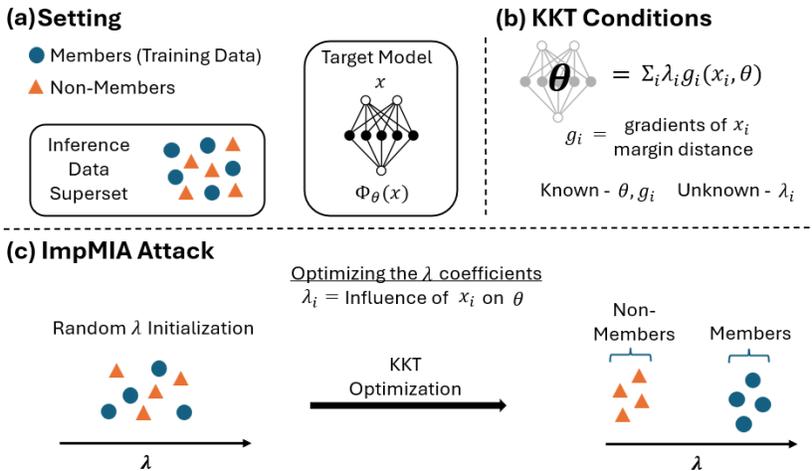
Figure 1: **Overview of the approach. (a)** *Setting: Given a trained model with parameters θ and a candidate superset containing training* members *(blue) and* non-members *(orange), the adversary's goal is to identify which samples are members.* **(b)** *KKT conditions: Our attack builds on implicit bias theory, which shows that gradient-based optimization converges to solutions satisfying the Karush–Kuhn–Tucker (KKT) conditions of the maximum-margin problem. Since weights are known and gradients are computable, only the coefficients remain unknown.* **(c)** *ImpMIA: We optimize one coefficient per sample to best reconstruct the model parameters, where members are expected to receive large coefficients and non-members small ones.*

current white-box attacks still fall short compared to the best black-box approaches when evaluated under stringent criteria such as the true-positive rate (TPR) at very low false-positive rates (FPR), which has been suggested as a reliable evaluation perspective by Carlini et al. (2022).

We propose *ImpMIA*, a white-box membership inference attack that is the first to adapt neural network implicit bias theory for this task (see our approach overview in Figure 1). Unlike prior approaches, our attack does not rely on reference models and is therefore unaffected by the common assumptions in reference-model methods. *ImpMIA* requires no knowledge of the target model's training procedure or data distribution, operating in a realistic scenario where only the model weights and a superset of the training data are available.

Our attack builds on the theory of implicit bias in neural networks, which shows that gradient-based optimization tends to converge to solutions that satisfy the Karush–Kuhn–Tucker (KKT) optimality conditions of a certain maximum-margin problem (Lyu & Li, 2019; Ji & Telgarsky, 2020). In practice, this implies that the trained parameters of a network can be approximately expressed as a linear combination of per-sample gradients from the training set. Given a set of candidate samples and the trained network weights, we optimize a set of coefficients—one for each sample—that best reconstructs the network parameters. This provides the key signal: training samples are expected to receive significantly larger coefficients, while non-members remain small.

ImpMIA achieves superior results, surpassing both black-box and white-box attacks under realistic settings across three benchmark datasets. Our extensive analysis shows that removing the knowledge assumptions made by most reference model based methods, leads to a significant drop in the performance of state-of-the-art methods, while our attack remains unaffected. Altogether, these results highlight the importance and effectiveness of our proposed method as a practical membership inference attack in realistic scenarios, likely to be most relevant for real-world applications.

Our contributions are as follows:

- We introduce *ImpMIA*, the first membership inference attack based on the implicit bias of gradient descent and its corresponding KKT conditions.

- *ImpMIA* achieves state-of-the-art performance in realistic scenarios where only model weights and a candidate data pool are available.

- We provide a systematic evaluation of the robustness of state-of-the-art MIA methods under realistic conditions where training hyperparameters, data distribution, or member ratios are unknown.

2 RELATED WORK

2.1 MEMBERSHIP INFERENCE

Membership Inference Attacks (MIAs) are typically divided into black-box attacks, which rely only on model outputs, and white-box attacks, which exploit access to model parameters.

White-box attacks exploit access to a model's internal parameters (often gradients) to amplify membership signals. Nasr et al. (2019) introduced one of the first frameworks, leveraging activations and per-example gradients. Sablayrolles et al. (2019) derived the Bayes-optimal test under white-box access, showing that maximum membership power can be achieved by computing likelihood ratios over model parameters. Leino & Fredrikson (2020) showed in their Stolen Memories attack that gradient norms alone provide strong membership signals, and that training an auxiliary classifier to distinguish gradients from members versus non-members further improves accuracy. Most recently, Cohen & Giryes (2024) proposed a self-influence attack that uses influence functions to measure each sample's effect on its own loss, combined with the predicted label. Another related work is IHA (Suri et al., 2024), an attack based on inverse–Hessian–vector products. However, this high-compute method restricts its evaluation to relatively small models on simple datasets and uses a different evaluation setting. While white-box access is a strong assumption, it is increasingly realistic as many modern models are released with their full weights (e.g., on Hugging Face).

Black-box MIAs assume the attacker can only query the target model and observe its outputs. One line of work is label-only attacks, which assume access only to predicted labels and infer membership from how labels change under small input perturbations (Choquette-Choo et al., 2021; Li & Zhang, 2021; Wu et al., 2024; Peng et al., 2024). While these attacks can be applied in any scenario, access to labels only provides significantly lower performance. Another line of work assumes access to the output logits rather than just labels. Shokri et al. (2017) introduced the shadow-model framework, training reference models to mimic the target and then learning an attack model from their outputs. Yeom et al. (2018) later showed that even without reference models, the simple "gap" heuristic—predicting membership when the model's output label matches the ground truth, can be effective. Li & Zhang (2021) proposed decision-based attacks relying on adversarial perturbations, while Ye et al. (2022) introduced *Attack-P*, a population-based loss thresholding method, and *Attack-R*, a sample-specific calibration using percentiles from reference models for improved robustness. Building on the reference-model paradigm, Carlini et al. (2022) proposed LiRA, which compares target losses to reference-model distributions and emphasized low false-positive evaluation. Zarifzadeh et al. (2023) (RMIA) further refined LiRA with an optimized likelihood-ratio test, improving efficiency under strict computational limits. LiRA and RMIA currently represent the strongest-performing black-box MIAs.

Limitations of Reference-Model Attacks. Reference-model attacks are costly to train and their effectiveness depends heavily on how these models are trained. Specifically, three key assumptions which violating them significantly reduces MIA performance: (i) *Knowledge of the target model's training hyperparameters* (e.g., learning rate, optimizer, epochs): Jayaraman et al. (2021b) and Carlini et al. (2022) (LiRA) reported accuracy drops when altering those hyperparmeters. (ii) *Matching data distribution*: Salem et al. (2019) and Shi et al. (2024) show degraded accuracy when shadows were trained on different domains (e.g., CIFAR-10 for a CIFAR-100 target). (iii) *Member ratio in the inference pool*: both Jayaraman et al. (2021b) and Song & Mittal (2021) found inflated false positives and reduced accuracy when this assumption was wrong. In this work, we systematically test these three factors showing significant drops across models on CIFAR-10, CIFAR-100, and CINIC-10. Such scenarios—where these factors are *unknown* to the attacker—are more realistic, as most models, particularly those trained on sensitive data, are unlikely to publish this information.

2.2 IMPLICIT BIAS OF GRADIENT DESCENT

In overparameterized neural networks, one might expect overfitting the training data. Yet gradient-based methods tend to converge to classifiers that generalize well to new unseen data (Zhang et al., 2021; Neyshabur et al., 2017). This phenomenon is explained by the *implicit bias* of training algorithms: gradient descent tends to prefer specific solutions, and characterizing these has been central to deep-learning theory in recent years (see Vardi (2023) for a survey). For homogeneous ReLU networks trained to zero logistic or cross-entropy loss, Lyu & Li (2019) and Ji & Telgarsky (2020) showed that the learned weights necessarily satisfy the *KKT conditions* of a maximum-margin prob-

lem. Building on this, Haim et al. (2022) demonstrated that networks trained with binary cross-entropy allow reconstruction of dozens of nearly pixel-perfect training samples. This was later extended to multiclass classifiers (Buzaglo et al., 2023) and more realistic transfer-learning work-flows (Oz et al., 2024). All of these data reconstruction attacks are limited to very small datasets (up to a few thousand examples), and require simple models (mostly MLPs). In this work, we adapt the implicit-bias approach for the first time to membership inference attack, identifying which samples from a candidate pool best satisfy the KKT conditions.

3 PRELIMINARIES

3.1 MEMBERSHIP INFERENCE ATTACKS SETTING

Membership inference attacks (MIAs) aim to determine which data points were part of the training set of a machine learning model. The strongest recent black-box methods are reference-model based, and they rely on additional assumptions about the target model's training configuration and the candidate set, which are unlikely to hold in practice. In this work, we focus on a realistic scenario where the adversary has access only to a superset that contains the training set and to the model weights. This reflects real-world conditions: modern models are often released publicly with their weights, while auditors may possess large candidate pools that include the training set but lack detailed knowledge of the training data distribution or the exact training configuration. Our setting adapts the basic membership inference game (Yeom et al., 2018; Jayaraman et al., 2021a), where a single sample is evaluated at a time, into a superset-based formulation in which the full candidate pool is attacked and evaluated (similar to the online setting in Carlini et al. (2022); Zarifzadeh et al. (2023)). We assume that the superset contains the full training set or at least a large portion of it. While this assumption was not taken in prior work, the reported results in those settings were in fact obtained under it. That is, for technical reasons, their evaluations were obtained in a setting where the attacker uses a superset of the training data (Carlini et al., 2022). Results for our method in a scenario where this assumption does not hold are presented in Appendix B.3.

Formally, we study a superset no auxiliary knowledge setting. Let X_{train} be the (unknown) training set drawn from a distribution $\mathcal{D}$, and f_θ a model trained on X_{train}. Let X_{sup} be a candidate pool such that $X_{\text{train}} \subseteq X_{\text{sup}}$, with the remaining samples being non-members, potentially drawn from other distributions. The adversary is given the trained parameters θ and the pool X_{sup}, but: (i) does not know the hyperparameters used to train the target model; (ii) cannot assume non-members are drawn from the same distribution as the training set; and (iii) does not know how many members are in X_{sup} or their ratio. The adversary must then assign a real-valued score to each sample, with membership decisions.

3.2 THE IMPLICIT BIAS FORMULATION

In this section, we provide an overview of the KKT conditions and the maximum-margin formulation, following the definitions in Haim et al. (2022); Buzaglo et al. (2023). While the theory described below is formally constrained to homogeneous[1] ReLU networks (Lyu & Li, 2019; Ji & Telgarsky, 2020), we show in practice that the results hold more generally for other architectures. The theoretical results of Lyu & Li (2019); Ji & Telgarsky (2020) consider training without weight decay, but in Appendix D we show that incorporating weight decay leads to the same final equations, and in Appendix B.5 we analyze its influence on the attack performance.

Implicit bias of gradient flow on homogeneous networks: Let $\Phi(\theta; \cdot) : \mathbb{R}^d \to \mathbb{R}^C$ be a homogeneous ReLU network with outputs $\Phi_j(\theta; x)$. Consider minimizing the cross-entropy loss over a multiclass dataset $\{(x_i, y_i)\}_{i=1}^n \subseteq \mathbb{R}^d \times [C]$ using gradient flow (i.e., gradient descent with a small step size). Suppose that at some time t_0 the network classifies all training samples correctly. Then gradient flow converges in direction to a KKT point of the multiclass maximum-margin problem:

$$\min_\theta \ \tfrac{1}{2}\|\theta\|^2 \quad \text{s.t.} \quad \Phi_{y_i}(\theta; x_i) - \Phi_j(\theta; x_i) \geq 1, \quad \forall i \in [n], \ \forall j \in [C] \setminus \{y_i\}.$$

The corresponding KKT conditions for solving this maximum margin problem are:

---

[1] A model Φ is homogeneous w.r.t. θ if there exists $L > 0$ such that $\forall c > 0, x : \ \Phi(x; c\theta) = c^L \Phi(x; \theta)$.

$$\theta - \sum_{i \in [n]} \sum_{j \in [C] \setminus \{y_i\}} \lambda_{i,j} \, \nabla_\theta \big[\Phi_{y_i}(\theta; x_i) - \Phi_j(\theta; x_i) \big] = 0, \tag{1}$$

$$\forall \, i \in [n], \; j \in [C] \setminus \{y_i\} : \begin{cases} \Phi_{y_i}(\theta; x_i) - \Phi_j(\theta; x_i) \; \geq \; 1, \\ \lambda_{i,j} \; \geq \; 0, \\ \lambda_{i,j} = 0 \; \text{if} \; \Phi_{y_i}(\theta; x_i) - \Phi_j(\theta; x_i) \neq 1. \end{cases} \tag{2}$$

Equation 1, called the *stationarity condition*, represents the weights as a linear combination of margin gradients (distance between a sample's true class Φ_{y_i} and other classes Φ_j), while Equation 2 specifies additional constraints. The coefficients are the $\lambda_{i,j}$, defined per sample i per class j. In practice, the distance of a sample x_i to the decision boundary is typically determined by a single competing class j. Therefore, following Buzaglo et al. (2023), we simplify the first condition by

considering only the class with the smallest margin:

$$\theta \; = \; \sum_{i=1}^{m} \lambda_i \, g_i, \quad g_i = \nabla_\theta \Big[\Phi_{y_i}(x_i; \theta) - \max_{j \neq y_i} \Phi_j(x_i; \theta) \Big]. \tag{3}$$

While our attack builds on the same condition as Buzaglo et al. (2023), our goal differs: instead of reconstructing training data $\{x_i\}$, we fix the candidate inputs and optimize only the coefficients $\{\lambda_i\}$ to obtain membership scores.

4 ImpMIA Attack

In this section, we introduce *ImpMIA*, our white-box membership inference attack that exploits the implicit bias of neural networks. The attack builds on the observation from Eq. 3 that trained parameters can be represented as a linear combination of per-sample gradients from the training samples (members). Thus, members can be distinguished from non-members by their relative contribution to this representation of the parameters, where members contribute to this reconstruction while non-members do not. We first outline the practical construction of the attack in Section 4.1, and then detail the technical optimization procedures and stabilization strategies in Section 4.2.

4.1 Practical Attack Construction

Building on the theoretical link between the KKT stationarity condition and the representation of trained parameters (Eq. 1), we now describe how this insight is used to devise the ImpMIA attack. The KKT stationarity condition guarantees that the trained parameter vector can be expressed as:

$$\theta = \sum_{i \in X_{\text{train}}} \lambda_i \, g_i,$$

where each g_i is the margin gradient of a training sample and $\lambda_i \geq 0$ is its corresponding multiplier. The model weights are known hence the per-sample gradients can be computed. Therefore, the only unknowns are the λ coefficients, which can be obtained by optimizing them to satisfy the equation.

In practice, the attacker does not know the true training set, but only has access to a candidate pool $X_{\text{sup}} = \{(x_i, y_i)\}_{i=1}^{M}$, which contains an unknown subset of training samples X_{train} and non-members X_{test}. However, we can still optimize the coefficients using all samples, deriving a λ coefficient for each (either member or not). This provides the key signal: we expect the coefficients of training samples to be significantly larger, while those of non-members remain small. This is because the number of network parameters is typically much larger than the size of the candidate pool, and therefore deriving the correct weights in the optimization is much more likely when true members exert stronger influence. Importantly, when $|X_{\text{sup}}|$ is smaller than the dimension of θ and the vectors $\{g_i\}$ are linearly independent, the system admits a unique solution for $\{\lambda_i\}$. Note that, following Eq. 2&3, we expect large coefficients for training samples near the margin (close to the decision boundary), while other samples are expected to have lower coefficients (zero in theory).

Formally, for each candidate (x_i, y_i) we compute the multiclass margin gradient

$$g_i = \nabla_\theta \Big[\Phi_{y_i}(\theta; x_i) - \max_{j \neq y_i} \Phi_j(\theta; x_i) \Big],$$

and stack these into the matrix $A = [g_1 \mid \cdots \mid g_M] \in \mathbb{R}^{p \times M}$, where p is the number of model parameters. If the training set were known, we could restrict to A_{train} and solve exactly for multipliers
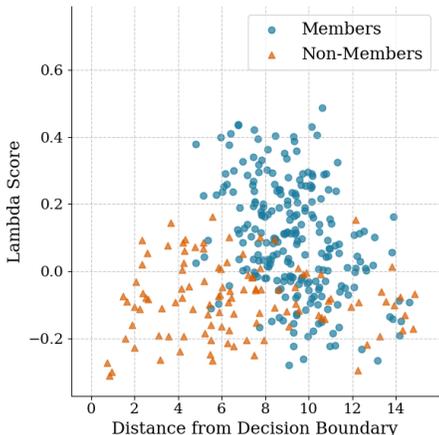
Figure 2: ***Lambda Scores Visualization.** Scatter plot of superset samples, with the x-axis showing distance to the decision boundary and the y-axis showing λ scores; points are colored by membership (member vs. non-member). High λ indicates membership.*
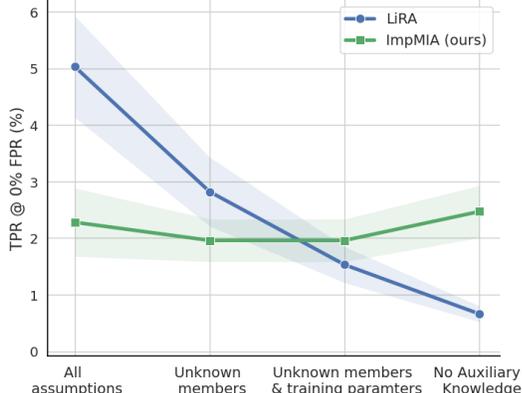
Figure 3: ***Effect of Assumption Removal.** Performance of the best prior method (LiRA) and our method (ImpMIA) under the progressive removal of assumptions on CINIC-10. LiRA degrades sharply as assumptions are removed, while ImpMIA maintains stable performance.*

λ_{train} such that $A_{\text{train}} \lambda_{\text{train}} = \theta$. Since the training set is unknown, we instead solve the full system $A \lambda_{\text{score}} = \theta$, deriving M (number of candidates) coefficients. The resulting coefficients are used to calculate a membership score, where large values for a specific sample are interpreted as evidence of a higher probability that this sample was part of the training data (i.e., a member). To improve robustness and suppress spurious large values from non-members, we incorporate additional techniques for regularization and aggregation (detailed in Section 4.2). In Figure 2, we present a scatter plot of members and non-members, where the y-axis shows the λ score and the x-axis the sample's distance from the margin (i.e., $\Phi_{y_i}(x_i; \theta) - \max_{j \neq y_i} \Phi_j(x_i; \theta)$). As illustrated, high λ scores are strong indicators of membership.

4.2 IMPLEMENTATION DETAILS

Given a set of training samples and their corresponding classes, we optimize the λ coefficients to satisfy the KKT conditions. We first filter out misclassified samples, since training members are more likely to be correctly predicted. For each remaining sample, we include both the original and its horizontal flip, reflecting the fact that most models are trained with augmentations, while keeping computational cost low by not adding further augmentations.

The only optimized variables are the λ coefficients. Therefore, we precompute the margin gradients with respect to the model parameters, forming the columns of the matrix A (as introduced in the previous section). Since A is extremely large (with the number of rows corresponding to the number of network parameters), we split it into blocks for more efficient optimization. Specifically, each block corresponds to roughly 1.5×10^5 parameters, and we optimize the coefficients separately per block. This block partitioning not only reduces memory usage, but also mitigates the ill-conditioning of A: consecutive layers or filters typically share similar statistics, so solving many smaller systems lowers the condition number compared to optimizing the full matrix at once. Moreover, although non-members can obtain a high coefficient due to imperfect optimization, deriving coefficient solutions per block allows averaging across blocks. This improves results, since a sample is unlikely to consistently receive high coefficients in different blocks if it was not part of the training set.

Both the gradient block and the target parameter vector are centered and normalized. For each sample, we then aggregate the optimized coefficients across blocks and augmentations to obtain a final score (see appendix A for more details). Our attack is designed to be both memory-efficient and numerically stable, while suppressing noisy scores for non-members.

5 EXPERIMENTAL SETTING

We evaluate **ImpMIA** against both black-box and white-box baselines across CIFAR-10, CIFAR-100, and CINIC-10, using a standard ResNet-18 as the target model. Our experiments are designed to reflect realistic adversarial conditions, where the attacker is given only the trained model weights

and a superset of candidate samples, with no knowledge of the training hyperparameters, data distribution, or member ratio. We first describe the datasets, evaluation metrics, and the competing baseline models (Section 5.1). We then detail the different scenarios corresponding to the assumptions usually made by reference-model–based MIAs, beginning with the setting where all assumptions are provided, and then moving to a more realistic setting without these assumptions (Section 5.2).

5.1 MODELS, DATASETS AND EVALUATION METRICS

For all experiments, the target model is a ResNet-18 trained following the standard recipe of Cohen & Giryes (2024). Specifically, we use a batch size of 100, a learning rate of 0.1, momentum 0.9 with Nesterov acceleration, weight decay of 10^{-4}, and train for 400 epochs using stochastic gradient descent (SGD) with standard data augmentations (random crop and horizontal flip). For each dataset and scenario, we randomly sampled 5 different sets of training samples, and trained 5 target models. Results are averaged across them.

We report performance using both aggregate metrics (AUC) and stringent low–false-positive criterion, True Positive Rate (TPR) at False Positive Rate (FPR) of 0.01% and 0.0%. This criterion introduced in Carlini et al. (2022), which observed that average-case metrics such as accuracy or AUC can be misleading: an attack may appear strong overall, yet fail completely in the regime of low false positives, which is the regime most relevant for privacy auditing (see Appendix F for a detailed discussion). In practice, an adversary cannot afford a large number of false alarms, as even a tiny FPR may translate to thousands of incorrectly flagged samples in real-world deployments. Therefore, evaluating TPR at very low FPR provides a stricter and more meaningful measure of membership inference risk.

We compare ImpMIA against recent state-of-the-art black-box and white-box membership inference attacks. For black-box attacks, we include Attack-P (Li & Zhang, 2021), Attack-R (Ye et al., 2022), and focused on the online version of LiRA (Carlini et al., 2022) and RMIA (Zarifzadeh et al., 2023), which currently represent the strongest black-box MIAs. For black-box baselines, we followed their best setting (e.g. training 256 reference models per experiment). For white-box attacks, we evaluate the adaptive self-influence attack (AdaSIF) (Cohen & Giryes, 2024), which represents the current state of the art in this category (see Appendix C.2 for additional implementation details). We also include as a baseline a simple white-box attack based on the magnitude of the network gradients, since Nasr et al. (2019) noted that this quantity provides the main signal in their attack (see Appendix C.2 for additional details). We were unable to compare with Nasr et al. (2019) and Leino & Fredrikson (2020), as their code is not available.

5.2 MEMBERSHIP INFERENCE ATTACK SCENARIOS

The basic scenario is the one commonly assumed in black-box attacks, which remain the strongest-performing methods even when compared to existing white-box approaches. In the *standard black-box setting*, the attacker is assumed to know both the model architecture and the training hyperparameters used to train the target model (e.g., learning rate, optimizer, number of epochs). The attacker is also given a pool of samples containing both members (training samples) and non-members, under the assumptions that (i) the pool is drawn from the same distribution as the training data and (ii) the member/non-member ratio is known, often fixed at 1:1.

These assumptions give reference-model attacks such as LiRA and RMIA a strong advantage: by training many reference models under the same conditions, they can effectively reconstruct the member/non-member loss distributions of the target model. This explains their strong performance in this regime, though it comes at the cost of training large model ensembles and relies on knowledge rarely available in practice.

To evaluate attack performance under more realistic conditions, we carefully design experimental scenarios that relax these assumptions. In Section 6, we present results in the more realistic setting where those assumptions are not made, as well as in each individual scenario where one assumption is removed. Importantly, to ensure fair comparison across scenarios and with prior work, we kept the target model fixed and followed the basic scenario used in previous studies.

The assumption-elimination scenarios are:

- *Unknown Training Configuration* – Since the attacker is not exposed to the target model's training parameters, we trained the reference models of methods that require them using different settings. Specifically, for the reference models we used a different batch size (200 instead of 100),

Table 1: **Membership Inference Results.** *Performance of ImpMIA compared to both black-box (LiRA, RMIA) and white-box baselines across three datasets under the realistic no auxiliary knowledge setting. The main relevant metrics are TPR values at fixed false-positive rates (FPR = 0.00% and 0.01%), which capture detection power under stringent error constraints. ImpMIA significantly surpasses all other methods by a wide margin, due to their reliance on the different assumptions. For completeness, we also report AUC as an aggregate measure.*

	CIFAR-10			CIFAR-100			CINIC-10		
Attack	**AUC**	**@0.01 %**	**@0.00 %**	**AUC**	**@0.01 %**	**@0.00 %**	**AUC**	**@0.01 %**	**@0.00 %**
Attack-P	0.76	0.02	0.00	0.89	0.01	0.00	0.83	0.01	0.00
Attack-R	0.74	0.23	0.04	0.95	0.52	0.04	0.83	0.31	0.00
LiRA	0.80	0.55	0.17	0.96	7.90	2.36	**0.88**	2.27	0.66
RMIA	0.80	0.19	0.01	**0.97**	6.73	1.22	0.87	0.15	0.03
GradNorm – loss	**0.81**	0.11	0.01	0.93	0.10	0.04	0.85	0.09	0.01
GradNorm – margin	0.72	0.02	0.00	0.81	0.02	0.01	0.77	0.03	0.01
AdaSIF	0.80	0.05	0.00	0.92	0.01	0.00	0.85	0.01	0.00
Ours	**0.81**	**2.76**	**1.41**	0.95	**14.86**	**5.26**	0.87	**5.32**	**2.47**

learning rate (0.01 instead of 0.1), weight decay (10^{-3} instead of 10^{-4}), and epochs (100 instead of 400) than those used for the ResNet-18 target model (detailed in Section 5.1).

- **Different Data Distribution** – In this case, the attacker's candidate pool mixes in-distribution data (the distribution from which the target model was trained) and out-of-distribution (OOD) data. For each dataset, we construct a pool of $50k$ samples by combining $30k$ in-distribution images with $20k$ OOD images (taken from another dataset). The target model is trained on $25k$ in-distribution samples drawn from the $30k$ portion, allowing for 5 repetitions of the experiment (with 5 different target models). In the reference-based attacks under the relevant online setting, the attacker trains each reference model on half of the superset, i.e., $25k$ examples sampled from the full mixed pool. OOD sources include a subset of ImageNet adapted to CIFAR-10 (CINIC-10 (Darlow et al., 2018)) and an enriched OpenImages dataset (Kuznetsova et al., 2020).

- **Unknown Fraction of Members** – In this case, the attacker does not know the proportion of training members in the candidate pool. The pool is constructed to contain $80k$ examples. Reference-model attacks that assume a 1:1 ratio train their reference models on $40k$ samples (half treated as members and half used to estimate the loss distribution of non-members), while the target model is trained on only $25k$. This mismatch causes the member/non-member loss distributions to differ significantly. We evaluate this scenario individually on CINIC-10, since the other datasets are too small for a meaningful setup.

- **No Auxiliary Knowledge** – Combining the above cases, the candidate pool for each dataset has $80k$ samples formed by mixing $30k$ in-distribution with $50k$ OOD images. The attacker trains reference models on a $40k$-example subset sampled from the full mixed pool under different configurations and without access to the true member ratio.

6 RESULTS

In this section, we quantitatively compare our *ImpMIA* attack against prominent prior black-box and white-box attacks across multiple datasets. In Section 6.1, we demonstrate the superiority of our attack in the realistic scenario where only the model weights are known and the attacker is given a superset of samples that includes the training data, but without any additional knowledge of the model training or the superset composition. Next, in Section 6.2, we systematically analyze the impact of eliminating each assumption across different models, showing that reference-model–based methods suffer significant performance drops, while our method remains unaffected. Further analysis of the method and ablation studies can be found in Appendix B.

6.1 MEMBERSHIP INFERENCE RESULTS

We report membership inference attack results across three datasets, demonstrating the superiority of our proposed attack in the realistic scenario described above (without assumptions on model training, data distribution, or member ratio). As shown in Table 1, reference-model attacks such as LiRA and RMIA struggle severely in this regime: at 0% False Positive Rate (FPR), LiRA achieves

Table 2: *Evaluation of Assumptions Influence. CINIC-10 membership inference across five scenarios: standard setting (all assumptions), removal of each assumption individually, and removal of all three simultaneously. Each entry shows TPR (%) at 0.01% / 0.00% FPR. The last column reports relative % of performance drop with respect to the Standard Setting.*

Method	Standard Setting	Unknown Training Config.	Different Distribution	Unknown Fraction of Members	No Auxiliary Knowledge
Attack-R	4.62 / 1.81	1.62 / 0.37	3.27 / 1.42	2.42 / 0.00	0.31 -93.3% / 0.00 -100%
LiRA	7.59 / 5.03	5.81 / 3.47	3.73 / 1.84	5.70 / 2.82	2.27 -70.1% / 0.66 -86.9%
RMIA	0.24 / 0.08	0.92 / 0.32	0.28 / 0.08	0.34 / 0.06	0.15 -37.5% / 0.03 -62.5%
ImpMIA (ours)	3.67 / 2.28	3.67 / 2.28	3.28 / 2.69	5.19 / 1.96	5.32 / 2.47

(TPR @ 0.01 / 0.00%)

only 0.17% True Positive Rate (TPR) on CIFAR-10, and RMIA 0.01% . Importantly, these are the best-performing attacks—even compared to white-box methods—when the knowledge assumptions are provided (see Table T7 in the appendix). Their effectiveness relies on training large sets of reference models under matching conditions, a requirement that breaks down when the attacker cannot replicate the target's training process. In contrast, *ImpMIA* avoids training reference models entirely, and maintains strong TPR at low FPR across all datasets. On CIFAR-10, our attack achieves 1.41% TPR at 0% FPR, and 2.76% at 0.01% FPR, with similar or larger gains on the other datasets. Our approach achieves substantially stronger performance at strict low-FPR operating points, which are the most relevant in practical membership inference scenarios, and comparable AUC results. We further present the FPR–TPR trade-off curves (ROC curves) for all three datasets in Figure S2. Importantly, our attack is computationally much cheaper than reference-based methods, as it does not require training reference models and is about 8× faster than reference-model attacks (see Appendix A).

6.2 Assumptions Influence Analysis

We present a detailed analysis of the influence of removing each assumption—individually and jointly—on attack performance. As discussed earlier, reference-model–based methods rely on training reference models under conditions that closely match the target model. Their effectiveness comes from approximating the loss distributions of members versus non-members, which requires alignment between target and reference training.

In Table 2 we report results on the CINIC-10 dataset across five scenarios: all assumptions provided ("Standard Setting"), the removal of each assumption individually, and the removal of all three assumptions simultaneously. As shown, all methods except our proposed *ImpMIA*—which does not rely on any reference models—suffer substantial drops in performance when all assumptions are removed. In particular, LiRA and Attack-R exhibit a clear degradation as assumptions are removed. While they perform well in the standard setting, their TPR at low FPR decrease substantially under unknown configuration, distribution shift, and unknown ratio. In contrast, our method achieves strong results in these settings, as it does not depend on such assumptions. We observed improvements in *ImpMIA* at 0.01% FPR level when the fraction of members was changed, which may be explained by the evaluation metric's dependence on the pool size (see Appendix B.6). It is worth noting that RMIA's performance in the standard setting is lower than those reported in its original paper. This is because our training follows the white-box setup from Cohen & Giryes (2024), which differs from RMIA's original experimental setting. This may imply limited generalization of RMIA (see Appendix C.1 for further discussion).

Figure 3 further visualizes the effect of assumption removal (for 0% FPR) in CINIC-10 dataset, for the top-performing method (LiRA) and our *ImpMIA*. As seen, being a reference-model–based method, LiRA degrades sharply as assumptions are removed, while *ImpMIA* shows no loss in performance. Overall, these results demonstrate the robustness and effectiveness of our approach for membership inference under realistic conditions where the attacker cannot rely on privileged training knowledge.

	VGG16			ResNet50		
Attack	**AUC**	**@0.01 %**	**@0.0 %**	**AUC**	**@0.01 %**	**@0.0 %**
LiRA	0.75	0.62	0.18	0.79	1.02	0.26
RMIA	**0.78**	0.69	0.06	0.78	0.09	0.02
Ours	**0.78**	**1.59**	**0.56**	**0.82**	**1.80**	**0.78**

Table 3: ***Membership Inference Results on Different Architectures.*** *Performance of LiRA, RMIA, and our method on VGG16 and ResNet50. We report AUC and TPR at fixed false-positive rates (FPR = 0.01% and 0.0%).*

7   ABLATION AND ANALYSIS

In this section, we discuss additional experiments analyzing our method. Further results and discussion can be found in appendix B.

Performance of our method on other architectures.   We conducted experiments in our setting comparing ImpMIA with the baselines on VGG16 and ResNet50 models trained on CIFAR-10 (see Table 3). ImpMIA shows a significant improvement over the other baselines on both architectures without any adaptation (we use the same hyperparameters for all models).

Evaluation on a large candidate pool.   We further evaluated the different attacks under the realistic setting with larger candidate pools. In our previous experiments, we used candidate pools of 50,000 ($\approx 2\times$ the training size) and 80,000 ($\approx 3\times$ the training size). To stress scalability, we also ran experiments with a candidate pool of 250,000 samples ($\approx 10\times$ the training size). We were unable to include RMIA due to its extremely high memory requirements in this setting. As can be seen in table T17, ImpMIA outperforms the other methods in this scenario as well.

Effect of training sample coverage in the superset.   Our method relies on linking training samples to the learned weights. Consequently, if a large portion of the training set is missing from the candidate set, performance naturally decreases (Table T2). In Table T3, we directly compare against the previous best methods under only 10% coverage in our realistic scenario. Even with this low coverage our results are comparable to the best competitors, and with higher coverage our method clearly surpasses them (Table 1).

Score thresholding using a reference non-member set.   We may want to explicitly control the score threshold used to decide which samples are members. In Figure S3, we show that we can select a threshold using a reference non-member set. We report two optimization runs: (i) coefficients optimized on a set containing only non-members (the reference non-member set), and (ii) coefficients optimized on a set containing only members. Even though these are optimized separately, a threshold chosen by fixing the tolerated number of false positives on the non-member set remains effective when applied to the member scores. Concretely, we can use a known set of non-members to choose a score threshold, and then apply this threshold to any candidate superset to decide which samples are members.

8   DISCUSSION & LIMITATIONS

ImpMIA advances membership inference by introducing a simple, theory-driven white-box attack that outperforms both black- and white-box baselines under realistic scenarios. By avoiding the need for reference models and leveraging implicit bias in neural network training, our approach provides a more practical and scalable way to audit privacy in machine learning systems. The main assumptions of our attack are access to model weights and to a candidate superset containing the training set. The first assumption is increasingly realistic as many modern models are publicly released with their full parameters, and the second is reasonable since our method's efficiency allows scaling to very large candidate pools without the need to train reference models (see Appendix B.2). While performance is strongest when most of the training set is included, we show that our attack also works well with partial training coverage (see Appendix B.3).

Our work is the first to demonstrate the implications of implicit bias theory for membership inference attacks. More broadly, it provides a concrete case study of how insights from implicit bias theory, which have largely been developed in idealized or small-scale settings, can be instantiated in practical machine learning tasks, going beyond theory and toy examples to real datasets, larger neural networks, and standard training regimes. *ImpMIA* provides a step forward in practical privacy auditing, establishing a bridge between implicit bias theory and applied machine learning.

REFERENCES

Gon Buzaglo, Niv Haim, Gilad Yehudai, Gal Vardi, Yakir Oz, Yaniv Nikankin, and Michal Irani. Deconstructing data reconstruction: Multiclass, weight decay and general losses. *Advances in Neural Information Processing Systems*, 36:51515–51535, 2023.

Nicholas Carlini, Steve Chien, Milad Nasr, Shuang Song, Andreas Terzis, and Florian Tramer. Membership inference attacks from first principles. In *2022 IEEE symposium on security and privacy (SP)*, pp. 1897–1914. IEEE, 2022.

Christopher A. Choquette-Choo, Florian Tramèr, Nicholas Carlini, and Nicolas Papernot. Label-only membership inference attacks. In *Proceedings of the 38th International Conference on Machine Learning*, volume 139 of *Proceedings of Machine Learning Research*, pp. 1964–1974. PMLR, 2021. URL https://proceedings.mlr.press/v139/choquette-choo21a.html.

Gilad Cohen and Raja Giryes. Membership inference attack using self influence functions. In *Proceedings of the IEEE/CVF Winter Conference on Applications of Computer Vision*, pp. 4892–4901, 2024.

Luke N Darlow, Elliot J Crowley, Antreas Antoniou, and Amos J Storkey. Cinic-10 is not imagenet or cifar-10. In *NeurIPS Workshop on Machine Learning Systems (MLSys)*, 2018.

Niv Haim, Gal Vardi, Gilad Yehudai, Ohad Shamir, and Michal Irani. Reconstructing training data from trained neural networks. *Advances in Neural Information Processing Systems*, 35:22911–22924, 2022.

Bargav Jayaraman, Lingxiao Wang, David Evans, Lee Gu, and Yinqian Hong. Revisiting membership inference under realistic assumptions. *Proceedings on Privacy Enhancing Technologies*, 2021(2):348–368, 2021a.

Bargav Jayaraman, Lingxiao Wang, David Evans, Lee Gu, and Yinqian Hong. Revisiting membership inference under realistic assumptions. *Proceedings on Privacy Enhancing Technologies*, 2021(2):348–368, 2021b.

Ziwei Ji and Matus Telgarsky. Directional convergence and alignment in deep learning. *Advances in Neural Information Processing Systems*, 33:17176–17186, 2020.

Alina Kuznetsova, Hassan Rom, Neil Alldrin, Jasper Uijlings, Ivan Krasin, Jordi Pont-Tuset, Shahab Kamali, Stefan Popov, Matteo Malloci, Alexander Kolesnikov, Tom Duerig, and Vittorio Ferrari. The open images dataset v4: Unified image classification, object detection, and visual relationship detection at scale. *International Journal of Computer Vision (IJCV)*, 128:1956–1981, 2020.

Klas Leino and Matt Fredrikson. Stolen memories: Leveraging model memorization for calibrated {White-Box} membership inference. In *29th USENIX security symposium (USENIX Security 20)*, pp. 1605–1622, 2020.

Zheng Li and Yang Zhang. Membership leakage in label-only exposures. In *Proceedings of the 2021 ACM SIGSAC Conference on Computer and Communications Security*, pp. 880–895, 2021.

Kaifeng Lyu and Jian Li. Gradient descent maximizes the margin of homogeneous neural networks. *arXiv preprint arXiv:1906.05890*, 2019.

Milad Nasr, Reza Shokri, and Amir Houmansadr. Comprehensive privacy analysis of deep learning: Passive and active white-box inference attacks against centralized and federated learning. In *2019 IEEE symposium on security and privacy (SP)*, pp. 739–753. IEEE, 2019.

Behnam Neyshabur, Srinadh Bhojanapalli, David McAllester, and Nati Srebro. Exploring generalization in deep learning. *Advances in neural information processing systems*, 30, 2017.

Yakir Oz, Gilad Yehudai, Gal Vardi, Itai Antebi, Michal Irani, and Niv Haim. Reconstructing training data from real world models trained with transfer learning. *arXiv preprint arXiv:2407.15845*, 2024.

Yuefeng Peng, Jaechul Roh, Subhransu Maji, and Amir Houmansadr. Oslo: One-shot label-only membership inference attacks. In *Advances in Neural Information Processing Systems*, NeurIPS 2024, 2024. doi: 10.52202/079017-1991. URL `https://proceedings.neurips.cc/paper_files/paper/2024/hash/71f88122d414cfeb455ac0ed932fbe1f-Abstract-Conference.html`.

Alexandre Sablayrolles, Matthijs Douze, Cordelia Schmid, Yann Ollivier, and Hervé Jégou. White-box vs black-box: Bayes optimal strategies for membership inference. In *International Conference on Machine Learning*, pp. 5558–5567. PMLR, 2019.

Ahmed Salem, Yang Zhang, Mathias Humbert, Pascal Berrang, Mario Fritz, and Michael Backes. Ml-leaks: Model and data independent membership inference attacks and defenses on machine learning models. In *Network and Distributed Systems Security Symposium (NDSS)*, 2019.

Yichuan Shi, Olivera Kotevska, Viktor Reshniak, and Amir Sadovnik. Assessing membership inference attacks under distribution shifts. In *Proceedings of the 2024 IEEE International Conference on Big Data (BigData)*, pp. 4127–4131. IEEE, 2024. doi: 10.1109/BigData62323.2024. 10825580.

Reza Shokri, Marco Stronati, Congzheng Song, and Vitaly Shmatikov. Membership inference attacks against machine learning models. In *2017 IEEE symposium on security and privacy (SP)*, pp. 3–18. IEEE, 2017.

Liwei Song and Prateek Mittal. Systematic evaluation of privacy risks of machine learning models. In *30th USENIX Security Symposium (USENIX Security 21)*, pp. 2615–2632, 2021.

Anshuman Suri, Xiao Zhang, and David Evans. Do parameters reveal more than loss for membership inference? *Transactions on Machine Learning Research (TMLR)*, 2024. URL `https://arxiv.org/abs/2406.11544`.

Gal Vardi. On the implicit bias in deep-learning algorithms. *Communications of the ACM*, 66(6): 86–93, 2023.

Yutong Wu, Han Qiu, Shangwei Guo, Jiwei Li, and Tianwei Zhang. You only query once: An efficient label-only membership inference attack. In *Proceedings of the International Conference on Learning Representations*, ICLR 2024, 2024. URL `https://openreview.net/forum?id=7WsivwyHrS`.

Jiayuan Ye, Aadyaa Maddi, Sasi Kumar Murakonda, Vincent Bindschaedler, and Reza Shokri. Enhanced membership inference attacks against machine learning models. In *Proceedings of the 2022 ACM SIGSAC conference on computer and communications security*, pp. 3093–3106, 2022.

Samuel Yeom, Irene Giacomelli, Matt Fredrikson, and Somesh Jha. Privacy risk in machine learning: Analyzing the connection to overfitting. In *2018 IEEE 31st computer security foundations symposium (CSF)*, pp. 268–282. IEEE, 2018.

Sajjad Zarifzadeh, Philippe Liu, and Reza Shokri. Low-cost high-power membership inference attacks. *arXiv preprint arXiv:2312.03262*, 2023.

Chiyuan Zhang, Samy Bengio, Moritz Hardt, Benjamin Recht, and Oriol Vinyals. Understanding deep learning (still) requires rethinking generalization. *Communications of the ACM*, 64(3):107–115, 2021.

Appendix

A ImpMIA Additional Implementation Details

In this section we provide further details on the implementation of our attack. The overall pipeline includes the following parts: (i) **pre-filtering** of candidate samples based on their classification margin, (ii) **augmentation** using horizontal flips, (iii) **block division** of weights for more efficient optimization, (iv) **gradient matrix construction** per block-structured gradient matrix A over the chosen model parameters, (v) **optimization** to solve the KKT conditions and learn the coefficients λ via blockwise optimization with dedicated regularization, (vi) **coefficient aggregation** across blocks into robust per-sample scores, and finally (vii) **post-processing** of the coefficient scores to derive the final per-sample score.

We first perform **pre-filtering**, where we filter out misclassified samples, since training members are more likely to be correctly predicted. For each candidate sample (x_i, y_i), we compute its logit margin:

$$\Delta_i = \Phi_{y_i}(\theta; x_i) - \max_{j \neq y_i} \Phi_j(\theta; x_i),$$

and discard those with $\Delta_i < 0$. For each remaining sample we apply **augmentation**, including both the original and its horizontal flip. This reflects the fact that most models are trained with augmentations, while keeping computational cost low by not adding further augmentations. Final scores are averaged across the augmented views of each sample.

Next is **block division**. To manage dimensionality and improve optimization, parameters are partitioned into blocks of $\sim 1.5 \times 10^5$ entries and solved one block at a time. For CIFAR-10 and CINIC-10 we include all layers, while for CIFAR-100 we restrict to the final convolutional stages, where membership signals are strongest (Nasr et al., 2019). Parameters are grouped by layer order, and filters inside each convolutional layer are grouped together, since weights from the same filter/layer share statistical properties such as sparsity and magnitude. This improves conditioning of the system. In the **gradient matrix construction** step, for each retained sample we compute the gradient of its margin w.r.t. the parameters and stack them as columns of a matrix $A \in \mathbb{R}^{p \times M}$. Both the gradient block and the target parameter vector are centered and normalized.

In the **optimization** step, for each block b with parameters $\theta_{(b)}$, we solve for coefficients $\lambda_{(b)}$ by minimizing:

$$\mathcal{L} = 1 - \cos\big(A_{(b)}\lambda_{(b)}, \theta_{(b)}\big) + \alpha\,\mathcal{L}_{\text{neg}} + \beta\,\mathcal{L}_{\text{marg}}.$$

Here, $\mathcal{L}_{\text{neg}}$ penalizes negative entries in $\lambda_{(b)}$ (reflecting complementary slackness of the KKT equations), and $\mathcal{L}_{\text{marg}}$ down-weights high-margin points, since low-margin training samples are more likely to be memorized (Haim et al., 2022). We use cosine similarity because it removes scale sensitivity and is more robust than ℓ_2 loss, preventing non-members from being incorrectly emphasized. Optimization uses AdamW with cosine learning-rate scheduling, gradient clipping, and early stopping. Coefficients are debiased by stored column norms and z-scored within each block.

After optimizing each block separately, we perform **coefficient aggregation**. Each block j yields a coefficient vector $\lambda^{(j)}$. For each sample i, we collect $\{\lambda_i^{(j)}\}_j$, sort them, and fuse into a robust score using a trimmed mean (averaging central values while discarding extremes) and a signal-to-noise ratio (SNR, mean over standard deviation across blocks). This suppresses spurious outliers and emphasizes consistent member signals.

Finally, in the *post-processing* step, we refine the raw scores using three components: ***(i) class-level margin boosting, (ii) sample-level margin boosting, and (iii) distance-based scaling***. Both boosting mechanisms adjust a sample's score according to its margin (distance from the decision boundary), but at different granularities (class vs. individual sample). ***(i) Class-level boosting*** is a simple per-class rescaling step, motivated by prior work (Nasr et al., 2019) showing that some classes are systematically more vulnerable to membership inference. Our boost builds on the observation that harder classes (with lower average margins) are more likely to memorize additional samples, so an attack can potentially recover more members from these classes. Accordingly, we assign slightly higher weight to harder classes and mildly downweight easier ones via a small per-class

scaling coefficient of 0.03. ***(ii) Sample-level margin boosting*** then refines scores within each class: following previous observations (e.g., Haim et al.) that near-boundary points are more likely to be memorized, we slightly upweight low-margin, near-boundary samples and mildly downweight very high-margin ones, using a per-sample scaling factor of 0.3. ***(iii) Distance-based scaling*** further penalizes deviation from the estimated class margin. We approximate the class margin $\bar{m}_c$ as the mean margin of the top-k highest-coefficient samples in each class, and rescale scores by dividing by $|\Delta_i - \bar{m}_c|^\eta$, where Δ_i is the margin of sample i and $\eta > 0$ controls how strongly this distance affects the rescaling (we set $\eta = 0.05$ in all experiments). This ensures that only samples whose margins are consistent with typical member behavior retain high scores, helping to reduce false positives among non-members.

Layer Selection for CIFAR-100. For CIFAR-10 and CINIC-10 we construct the gradient matrix A from all convolutional layers of the network. For CIFAR-100, however, we restrict A to the final convolutional stages. This choice is motivated by both prior work and empirical observations. Nasr et al. (2019) empirically observed that, in deep CNNs trained on CIFAR-100, the strongest membership signals reside in the gradients of the later layers, while earlier layers mostly learn generic low- and mid-level features that generalize well and leak relatively little membership information. In a many-class regime such as CIFAR-100, early and mid-level layers must be heavily shared across classes, whereas the final convolutional blocks and classifier head implement sharp, class-specific decision boundaries and absorb most of the memorization.

Hyperparameter Selection. All hyperparameters of *ImpMIA* were selected using a held-out evaluation set. For CIFAR-10 and CINIC-10 we used a dedicated validation split constructed from CINIC-10, which is large enough to provide an independent validation pool. For CIFAR-100 we used a validation split taken from the generated candidate set. For each dataset, we followed the same protocol as in our main experiments: we trained 5 target models with different random seeds (affecting both the data split and the initialization) under the realistic "no auxiliary knowledge" setting, and ran *ImpMIA* for a small grid of hyperparameter configurations. We then selected the configuration that achieved the best average performance across these 5 runs according to our main evaluation criteria (TPR at low FPR). The same hyperparameters are used across all scenarios and across all architectures (ResNet-18, VGG16, and ResNet50).

Running Time. Training our proposed attack (*ImpMIA*) takes about 24 hours on a single H100 GPU, or 3 hours when distributed across 8 GPUs. In contrast, black-box reference-model attacks require about 8 days on a single GPU, or 1 day on 8 GPUs.

14

B ADDITIONAL ABLATION AND ANALYSIS

In this section, we provide further ablations and analyses of our approach: (i) visualization of the λ scores across different classes (see Appendix B.1); (ii) the ability to apply our attack on large candidate pools (see Appendix B.2) ; (iii) the effect of the number of training samples included in the superset (see Appendix B.3); (iv) ablations on the different scoring variants used in our method (see Appendix B.4); (v) the influence of weight decay on the results, showing that our method also works without explicit weight decay (see Appendix B.5); (vi) the effect of candidate pool size on evaluation (see Appendix B.6) and (vii) the influence of pre-filtering on performance (see Appendix B.7).

B.1 VISUALIZATION OF λ SCORES.

In Figure S1, we present results for six different CIFAR-100 classes. The plots show the λ score on the y-axis and the distance from the margin on the x-axis. As expected, high λ scores are strong indicators of membership. Samples very close to the margin are more likely to be non-members, while almost all members with high λ values fall slightly farther from the margin. This is consistent with the fact that models are trained to push training samples away from the margin, while hard test samples can lie closer to it. Interestingly, training samples that remain close to the margin are those that the network tends to memorize (Haim et al., 2022), and therefore receive higher λ scores, reflecting their strong influence on the model's predictions and weights.
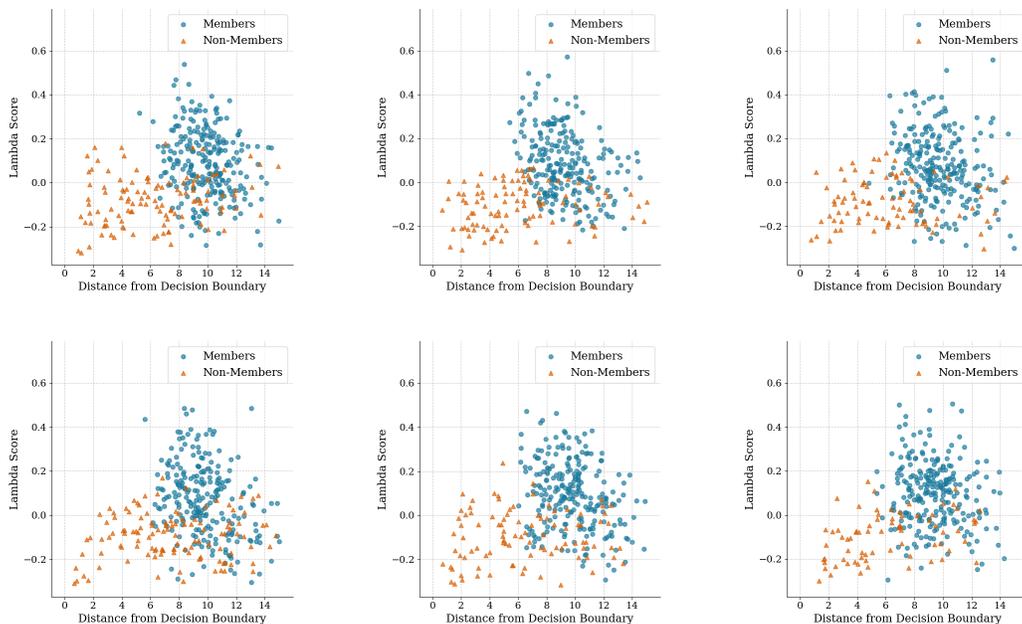

Figure S1: ***Lambda Scores Visualization (CIFAR-100).*** *Scatter plots for six different classes. Each plot shows superset samples; x-axis is distance from the decision boundary, y-axis is the λ score, and points are colored by membership (member vs. non-member). High λ values strongly indicate membership.*

B.2 LARGE CANDIDATE POOL

We further evaluated ImpMIA under larger candidate pools. In addition to the $50,000$ ($\approx 2\times$) and $80,000$ ($\approx 3\times$) candidate sets reported in the main text, we consider a pool of $250,000$ candidates ($\approx 10\times$ the training size) on CIFAR-10. Following our realistic no auxiliary knowledge protocol, the target model is trained on $25,000$ CIFAR-10 samples, while the reference set consists of the remaining $25,000$ CIFAR-10 samples together with $200,000$ images from CINIC-10. As shown in Table T17, ImpMIA achieves TPRs of 3.00% at 0.01% FPR and 0.54% at 0.00% FPR, substantially outperforming other MIAs at low FPRs in the larger candidate pool scenario.

Attack	AUC	@0.01 %	@0.00 %
Attack-R	0.75	0.01	0.00
Attack-P	0.76	0.12	0.00
LiRA	**0.80**	0.54	0.11
Ours	0.79	**3.00**	**0.54**

Table T1: ***Membership inference with a 250K candidate pool (CIFAR-10).*** *We compare ImpMIA to other MIA baselines under the realistic no auxiliary knowledge setting. We report AUC and TPR at fixed false-positive rates (FPR = 0.01% and 0.00%).*

B.3 EFFECT OF TRAINING SAMPLE COVERAGE IN THE SUPERSET

Our method relies on the implicit bias of the network, linking training samples to the learned weights. Consequently, if a large portion of the training set is missing from the candidate superset, performance naturally decreases. Importantly, in practice it is reasonable to expect supersets that cover most of the training set, especially since our method's efficiency allows scaling to very large candidate pools without the need to train reference models. As shown in Table T2, for the standard setting performance is strongest when most of the training set is included, but our attack also works well under partial training coverage. In all cases, evaluation is on a random $5,000$ (10%) samples from the candidate pool to avoid influence from candidate pool size on the reported metrics.

In Table T3 we show a direct comparison with the previous best methods under only 10% coverage in our realistic scenario. Even with this low coverage, our results are comparable to the best competitors, and with higher coverage our method clearly surpasses them (Table 1). Higher coverage is a likely scenario in many practical settings: in the real world, the attacker often has access to large candidate pools (for example, all publicly available images in a given domain), and our method's efficiency allows scaling to such large pools without training reference models.

	CIFAR-10		
Coverage	AUC	@0.1 %	@0.0 %
100%	0.72	5.13	2.63
75%	0.71	3.63	2.20
50%	0.70	3.10	1.45
25%	0.66	2.15	1.21
10%	0.62	1.54	0.39

Table T2: ***Effect of Training Sample Coverage (standard setting).*** *Ablation study on CIFAR-10 showing the impact of training sample coverage within the candidate superset. Performance is strongest when most of the training set is included, but our method remains effective under partial coverage.*

Attack	AUC	@0.1 %	@0.0 %
Attack-P	0.76	0.38	0.06
Attack-R	0.74	1.73	0.32
LiRA	**0.80**	2.98	**1.20**
RMIA	**0.80**	2.43	0.14
Ours	0.75	**3.01**	0.94

Table T3: ***Comparison under limited coverage of 10% (no auxiliary knowledge).*** *We compare our method on CIFAR-10 with previous attacks when the candidate superset covers only 10% of the training data in our realistic no auxiliary knowledge setting. Even under this low coverage, our results are comparable to the best competitors.*

B.4 Scoring Variants Ablation

We presents an ablation study of the different score-refinement components in our pipeline for CIFAR-10 in our realistic settings (see Table T4). After block-wise optimization, each sample has multiple coefficient estimates—one per block—which are fused into a robust score using both a trimmed mean (to discard extreme outliers) and a signal-to-noise ratio (SNR, mean over standard deviation across blocks). This aggregation step already improves robustness by emphasizing consistent membership signals. On top of this, we evaluate margin-based boosting and distance scaling. Class-level boosting gives higher weight to harder classes (with lower average margins), while per-sample boosting highlights points near the decision boundary, which are more likely to be memorized. Finally, distance scaling penalizes samples whose margins deviate from the estimated class margin, reducing false positives. As shown, each component contributes to performance gains, and the full *ImpMIA* pipeline achieves the strongest low-FPR detection. Moreover, with either aggregation option, and even without any post-processing, our attack already outperforms previous attacks and shows strong results. The post-processing steps have only a comparatively small influence at low FPR (e.g., TPR@0.00% ranges only from 1.23 to 1.41), while aggregation has a larger effect. This is expected, since aggregation determines how we exploit the main signal produced by the KKT-based optimization. Overall, the primary source of our gains comes from the implicit-bias-based optimization itself rather than from the specific post-processing.

Variant	AUC	@0.01 %	@0.0 %
Trimmed mean only	0.74	2.58	1.18
Robust SNR only	**0.85**	2.51	0.89
Fusion (trimmed mean + SNR)	0.82	2.60	1.23
+ Boost1 (class-level margins)	0.82	2.59	1.23
+ Boost2 (sample-level margins)	0.81	2.69	1.39
+ Trim division	0.82	**2.84**	1.31
ImpMIA	0.81	2.76	**1.41**

Table T4: ***Ablation of Imp-MIA Components (no auxiliary knowledge setting) for CIFAR-10.*** *Performance of different scoring variants and incremental boosts. We report AUC and TPR at fixed false-positive rates (FPR = 0.01% and 0.0%).*

B.5 Weight Decay Influence

To study the effect of explicit weight decay, we evaluated *ImpMIA* across several decay levels as well as without decay. While the KKT stationarity formulation applies in the homogeneous case, prior theory suggests that in non-homogeneous networks explicit weight decay is needed as a replacement. However, our results show that even in this setting the attack remains effective without weight decay. Interestingly, smaller decay values (e.g., 10^{-6}, 10^{-5}) tend to improve performance compared to larger ones, reflecting a balance between stability and memorization. Moreover, the case without weight decay performs comparably—and in some metrics slightly better—than with decay, consistent with the intuition that stronger regularization reduces memorization and weakens membership signals. This demonstrates both the robustness of our method and that weight decay is not strictly necessary for strong empirical performance.

Variant	CIFAR-10		
	AUC	@0.01 %	@0.0 %
Without weight decay	0.70	1.69	0.99
10^{-6}	0.71	1.73	0.93
10^{-5}	0.70	2.04	1.09
$\mathbf{10^{-4}}$	0.71	1.48	0.90

Table T5: ***Effect of Weight Decay.*** *Ablation on CIFAR-10 showing performance across different levels of weight decay, as well as without it. Although implicit bias theory assumes weight decay for the KKT characterization, our results show the attack remains effective regardless. Smaller decay values yield stronger performance, and even the no–weight decay case performs competitively, likely because stronger decay suppresses memorization signals.*

B.6 INFLUENCE OF NON-MEMBER RATIO ON EVALUATION

Our assumption-removal analysis also showed the influence of candidate pool size on model performance. In this setting, we lowered the member ratio by adding more non-members to the superset (increasing from 25K to 55K non-members). While our method does not rely on any specific member-to-non-member ratio, adding more non-members can affect results in two ways: (i) it increases the number of samples, which may make it harder to classify members, and (ii) it directly affects the evaluation metric, since FPR is defined relative to the total number of non-member samples. The overall performance reflects the interaction of these two factors. On the one hand, a larger pool introduces more distractors, potentially reducing accuracy. On the other hand, at fixed FPR thresholds (e.g., 0.01%), a larger pool allows more absolute mistakes. For instance, with 25K non-members, 0.01% FPR corresponds to only two false positives, whereas with 55K non-members, it allows up to five. Since coefficients are not uniformly distributed, permitting more mistakes can yield a nonlinear gain in TPR. In practice, we observed that at 0.01% FPR, our method performed better with 55K non-members than with 25K. This suggests that the positive effect of the evaluation metric outweighs the negative impact of additional distractors. Importantly, at 0% FPR—where the metric is unaffected by pool size—the results remained stable, as expected.

B.7 INFLUENCE OF PRE-FILTERING

The pre-filtering step aims to both stabilize the optimization by eliminating samples that are unlikely to be members (and therefore may add noise) and speed up optimization by having fewer samples. On the other hand, it may discard data points that are hard to learn even though they were in the training data, and therefore miss member samples. Since any attack is likely to miss some members, this is a trade-off that can be chosen in practice. We conducted an analysis of the influence of the pre-filtering step on our method's performance on CIFAR-10 for a single seed. In CIFAR-10 it filters out between 4–25% of the examples, depending on the seed and scenario. Results show a slight increase when using pre-filtering in AUC (0.78 to 0.80) and TPR at 0.01% FPR (3.2 to 3.44), and a slight decrease in TPR at 0.00% FPR (1.55 to 1.22). Overall, the pre-filtering step does not appear to have a significant influence on performance, but it does speed up optimization since fewer points are optimized (see Table T6).

Table T6: ***Effect of pre-filtering on ImpMIA (CIFAR-10, single seed).*** *Comparison of AUC and TPR at very low FPR with and without the pre-filtering step. We report AUC and TPR at fixed false-positive rates (FPR = 0.01% and 0.00%).*

Variant	AUC	@ 0.01% FPR	@ 0.00% FPR
No pre-filtering	0.78	3.20	1.55
With pre-filtering	0.80	3.44	1.22

C COMPETITIVE BASELINES: TECHNICAL DETAILS

C.1 BLACK-BOX BASELINES

For black-box comparisons, we used the official **RMIA** implementation, which also includes code for **LiRA**, **Attack-P**, and **Attack-R**. We ran the *full-power* RMIA variant described by Zarifzadeh et al. (2023), which trains 256 reference models per dataset, and used the same framework to evaluate the other black-box baselines. To ensure consistency, we adapted the code to match the training configuration of Cohen & Giryes (2024) (SIF): ResNet-18 backbone, inputs normalized to $[0, 1]$, and standard augmentations (random crop and horizontal flip).

RMIA requires dataset-specific configurations, which we followed exactly as provided in their code and paper for CIFAR-10, CIFAR-100, and CINIC-10. All experiments were therefore run with the recommended hyperparameters for each dataset. We emphasize that RMIA, despite reporting state-of-the-art results in its original paper, is highly sensitive to training configurations—especially at very low false-positive rates. Even minor mismatches in normalization, architecture, optimizer, or learning-rate schedule caused severe degradation in our experiments.

C.2 WHITE-BOX BASELINES

Gradient-based Baselines.   (Nasr et al., 2019) showed that the most informative white-box membership signal is the magnitude of per-sample gradients, since stochastic gradient descent drives member gradients toward zero. Building on this, we evaluate two baselines: (i) a *loss-gradient* score based on the norm $\|\nabla_\theta L(f(x), y)\|$, and (ii) a *margin-gradient* score based on the gradient $\|\nabla_\theta[f_y(x) - \max_{j\neq y} f_j(x)]\|$. For each sample (and its horizontal flip), we compute per-layer gradient norms, convert them into rank-based scores (higher rank = smaller norm), and average across layers and augmentations. The loss-gradient baseline directly instantiates Nasr et al. (2019) observation, while the margin-gradient baseline adapts it to sensitivity around the decision boundary, making it conceptually closer to *ImpMIA*.

SIF Attack.   The self-influence function (SIF) attack of Cohen & Giryes (2024) achieved state-of-the-art white-box membership inference in their paper, particularly under strong augmentations where gradient-norm methods fail. SIF measures a sample's effect on its own loss by approximating the influence function via recursive Hessian–vector products. Membership is inferred by whether a correctly classified sample's score lies close to zero, since training points tend to cluster tightly around this value while non-members yield more extreme values.

The original SIF formulation assumes access to labeled calibration samples to set the decision thresholds, and results were reported only on small subsets of data (500 calibration, 2,500 evaluation), producing binary member/non-member predictions. In our setting, however, no labeled calibration samples are available, and we require continuous membership scores to compute TPR at low FPR across the full evaluation pool. We therefore adapt the method with a simple *distance-to-zero* criterion: the closer a score is to zero, the stronger the evidence of membership. To stabilize the Hessian inversion, we use four recursion steps and average over four stochastic estimates. This reduced setting makes the attack faster while remaining stable across the full evaluation pool.

C.3 ADDITIONAL RESULTS

(a) CIFAR-10

(b) CIFAR-100

(c) CINIC-10
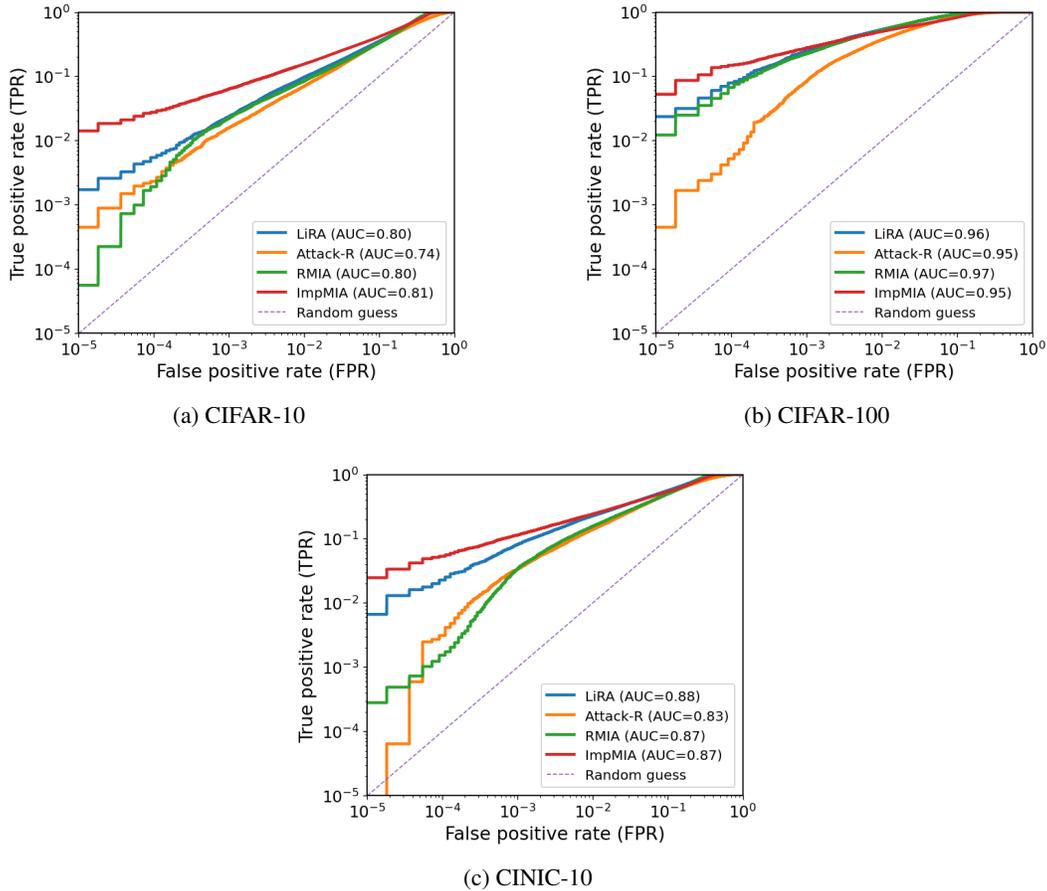
Figure S2: **TPR–FPR plots for the no auxiliary knowledge setting.** *These curves illustrate attack performance when the attacker faces realistic uncertainty: (i) training hyperparameters are unknown, (ii) the candidate pool mixes in- and out-of-distribution samples (distribution shift), and (iii) the fraction of members is unknown. The plots complement the main text by showing the full ROC behavior, especially in the low-FPR regime.*
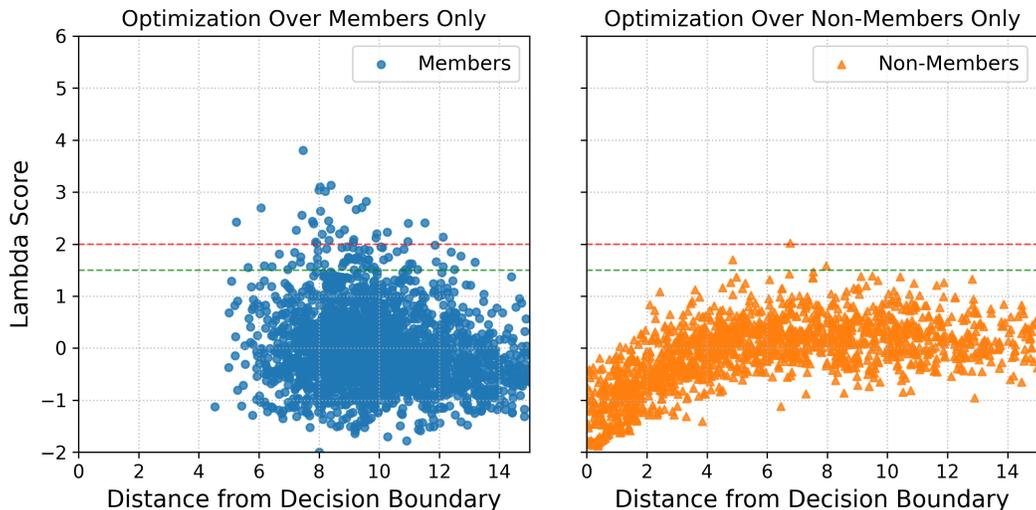
Figure S3: ***Behavior when the superset contains only members or only non-members.*** *We plot the learned λ scores when the coefficients are optimized on (i) a superset containing only non-members (which can be a reference non-member set), and (ii) a superset containing only members. Even though these optimizations are performed separately, many member samples still receive higher λ scores than non members.*

Table T7: ***Membership Inference Results (All Assumptions).*** *Performance across all datasets under the standard assumption-rich setting where training hyperparameters, data distribution, and member ratio are known. Metrics reported are TPR (%) at 0.00% and 0.01% FPR, with AUC included for completeness.*

	CIFAR-10			CIFAR-100			CINIC-10		
Attack	**AUC**	**@0.01 %**	**@0.0 %**	**AUC**	**@0.01 %**	**@0.0 %**	**AUC**	**@0.01 %**	**@0.0 %**
Attack-P	0.59	0.01	0.00	0.81	0.00	0.00	0.70	0.00	0.00
Attack-R	0.67	2.56	1.58	0.88	19.04	16.07	0.78	4.62	1.81
LiRA (online)	**0.75**	**5.28**	**3.56**	**0.95**	24.26	15.25	**0.86**	**7.59**	**5.03**
LiRA (offline)	0.58	1.94	0.74	0.81	5.88	2.44	0.69	2.59	1.17
RMIA (online)	0.74	1.48	0.69	0.94	14.69	8.46	0.84	0.24	0.08
RMIA (offline)	0.73	3.47	1.83	0.93	**25.98**	**20.44**	0.83	0.24	0.10
GradNorm − loss	0.61	0.01	0.00	0.83	0.01	0.00	0.74	0.00	0.00
GradNorm − margin	0.59	0.00	0.00	0.72	0.04	0.01	0.69	0.01	0.00
AdaSIF	0.62	0.01	0.00	0.87	0.03	0.01	0.75	0.00	0.00
Ours	0.71	1.48	0.90	0.90	9.66	6.73	0.82	3.67	2.28

Table T8: *Membership Inference Results (Unknown Member Fraction).* *CINIC-10 results when the attacker does not know the proportion of training members in the candidate pool. Metrics reported are TPR (%) at 0.00% and 0.01% FPR, plus AUC.*

	CINIC-10		
Attack	**AUC**	**@0.01 %**	**@0.0 %**
Attack-P	0.71	0.01	0.00
Attack-R	0.76	2.42	0.00
LiRA (online)	**0.85**	**5.70**	**2.82**
LiRA (offline)	0.58	0.41	0.12
RMIA (online)	0.83	0.34	0.06
RMIA (offline)	0.83	0.41	0.07
Ours	0.81	5.19	1.96

Table T9: *Membership Inference Results (Different Distribution).* *Performance across all datasets when the candidate pool mixes in-distribution and out-of-distribution data. Metrics reported are TPR (%) at 0.00% and 0.01% FPR, with AUC included for completeness.*

	CIFAR-10			CIFAR-100			CINIC-10		
Attack	**AUC**	**@0.01 %**	**@0.0 %**	**AUC**	**@0.01 %**	**@0.0 %**	**AUC**	**@0.01 %**	**@0.0 %**
Attack-P	0.75	0.03	0.00	0.90	0.02	0.00	0.82	0.01	0.00
Attack-R	0.71	1.02	0.63	0.93	10.10	4.95	0.82	3.27	1.42
LiRA (online)	**0.81**	1.94	1.14	**0.97**	12.66	4.63	**0.90**	**3.73**	1.84
LiRA (offline)	0.53	0.04	0.01	0.76	0.00	0.00	0.70	0.31	0.17
RMIA (online)	0.80	0.34	0.05	**0.97**	10.83	5.54	0.88	0.28	0.08
RMIA (offline)	0.79	0.56	0.14	**0.97**	**15.36**	**8.50**	0.86	0.51	0.15
Ours	**0.81**	**2.14**	**1.18**	0.95	11.60	5.05	0.85	3.28	**2.69**

Table T10: *Membership Inference Results (Unknown Training Configuration).* *Performance across all datasets when the attacker does not know the target model's training hyperparameters. Metrics reported are TPR (%) at 0.00% and 0.01% FPR, with AUC included for completeness.*

	CIFAR-10			CIFAR-100			CINIC-10		
Attack	**AUC**	**@0.01 %**	**@0.0 %**	**AUC**	**@0.01 %**	**@0.0 %**	**AUC**	**@0.01 %**	**@0.0 %**
Attack-P	0.59	0.01	0.00	0.81	0.01	0.00	0.71	0.00	0.00
Attack-R	0.67	1.53	0.49	0.90	2.97	1.55	0.79	1.62	0.37
LiRA (online)	**0.73**	**2.56**	**1.32**	0.92	13.86	9.93	**0.85**	**5.81**	**3.47**
LiRA (offline)	0.62	0.98	0.38	0.88	5.43	2.26	0.72	1.69	1.03
RMIA (online)	0.72	1.65	0.46	0.93	6.49	0.84	0.84	0.92	0.32
RMIA (offline)	0.71	1.89	0.76	0.92	**15.14**	**9.99**	0.83	0.79	0.08
Ours	0.71	1.48	0.90	0.90	9.66	6.73	0.82	3.67	2.28

22

Table T11: ***LiRA and RMIA: Offline vs. Online under No-Assumptions.*** *Results for LiRA and RMIA across all datasets in the realistic no-assumptions setting. The offline variant trains reference models independently of the candidate superset, while the online variant trains reference models directly on subsets of the superset, closer to the evaluation setup. Metrics reported are TPR (%) at 0.00% and 0.01% FPR, with AUC included for completeness.*

	CIFAR-10			CIFAR-100			CINIC-10		
Attack	**AUC**	**@0.01 %**	**@0.00 %**	**AUC**	**@0.01 %**	**@0.00 %**	**AUC**	**@0.01 %**	**@0.00 %**
LiRA (online)	**0.80**	**0.55**	**0.17**	0.96	**7.90**	**2.36**	**0.88**	2.27	0.66
LiRA (offline)	0.49	0.00	0.00	0.76	0.00	0.00	0.64	0.04	0.02
RMIA (online)	**0.80**	0.19	0.01	**0.97**	6.73	1.22	0.87	0.15	0.03
RMIA (offline)	0.79	0.26	0.00	**0.97**	7.35	1.67	0.86	0.11	0.02

Table T12: ***Membership Inference Results (No Assumptions).*** *Performance across all datasets under the realistic no-assumptions setting. Metrics reported are TPR (%) at 0.00% and 0.01% FPR, with standard error included. This table shows the same results as in Table 1, but with standard error values reported.*

	CIFAR-10		CIFAR-100		CINIC-10	
Attack	**@0.01 %**	**@0.0 %**	**@0.01 %**	**@0.0 %**	**@0.01 %**	**@0.0 %**
Attack-P	0.02 ± 0.00	0.00 ± 0.00	0.01 ± 0.00	0.00 ± 0.00	0.01 ± 0.00	0.00 ± 0.00
Attack-R	0.23 ± 0.10	0.04 ± 0.04	0.52 ± 0.14	0.04 ± 0.01	0.31 ± 0.19	0.00 ± 0.00
LiRA	0.55 ± 0.09	0.17 ± 0.01	7.90 ± 0.79	2.36 ± 0.30	2.27 ± 0.25	0.66 ± 0.13
RMIA	0.19 ± 0.04	0.01 ± 0.00	6.73 ± 0.84	1.22 ± 0.45	0.15 ± 0.02	0.03 ± 0.00
GradNorm–loss	0.11 ± 0.01	0.01 ± 0.00	0.10 ± 0.02	0.04 ± 0.01	0.09 ± 0.02	0.01 ± 0.00
GradNorm–margin	0.02 ± 0.01	0.00 ± 0.00	0.02 ± 0.01	0.01 ± 0.00	0.03 ± 0.00	0.01 ± 0.01
AdaSIF	0.05 ± 0.01	0.00 ± 0.00	0.01 ± 0.00	0.00 ± 0.00	0.01 ± 0.00	0.00 ± 0.00
ImpMIA (ours)	2.76 ± 0.34	1.41 ± 0.29	14.86 ± 0.40	5.26 ± 1.01	5.32 ± 0.42	2.47 ± 0.46

Table T13: ***Assumptions Influence (CINIC-10, @0.01% FPR).*** *Each entry is TPR (%) $\pm$ se. This table shows the same results as in Table 2, but with standard error values reported.*

Method	Standard Setting	Unknown Config	Different Distribution	Unknown Member Ratio	No Assumptions
Attack-R	4.62 ± 0.76	1.62 ± 0.67	3.27 ± 0.53	2.42 ± 0.19	0.31 ± 0.20
LiRA	7.59 ± 0.47	5.81 ± 0.53	3.73 ± 0.70	5.70 ± 0.58	2.27 ± 0.25
RMIA	0.24 ± 0.05	0.92 ± 0.32	0.28 ± 0.15	0.34 ± 0.06	0.15 ± 0.02
ImpMIA (ours)	3.67 ± 0.95	3.67 ± 0.95	3.28 ± 0.41	5.19 ± 0.31	5.32 ± 0.42

Table T14: ***Assumptions Influence (CINIC-10, @0.00% FPR).*** *Each entry is TPR (%) $\pm$ se. This table shows the same results as in Table 2, but with standard error values reported.*

Method	Standard Setting	Unknown Config	Different Distribution	Unknown Member Ratio	No Assumptions
Attack-R	1.81 ± 0.55	0.37 ± 0.26	1.42 ± 0.80	0.00 ± 0.00	0.00 ± 0.00
LiRA	5.03 ± 0.89	3.47 ± 1.01	1.84 ± 0.53	2.82 ± 0.61	0.66 ± 0.14
RMIA	0.08 ± 0.03	0.32 ± 0.09	0.08 ± 0.03	0.06 ± 0.03	0.03 ± 0.01
ImpMIA (ours)	2.28 ± 0.60	2.28 ± 0.60	2.69 ± 0.53	1.96 ± 0.38	2.47 ± 0.46

D   BINARY CASE OF THE KKT EQUATIONS AND IMPLICIT BIAS WITH WEIGHT DECAY

For completeness, we also present the implicit bias of neural networks for the binary classification case, as appeared in Lyu & Li (2019); Ji & Telgarsky (2020); Haim et al. (2022), and its extension to training with weight decay that was previously considered in (Buzaglo et al., 2023).

Implicit bias of gradient flow in homogeneous networks: Let $\Phi(\theta; \cdot) : \mathbb{R}^d \to \mathbb{R}$ be a homogeneous ReLU network. Consider minimizing the logistic loss over a binary classification dataset $\{(x_i, y_i)\}_{i=1}^{n} \subseteq \mathbb{R}^d \times \{\pm 1\}$ using gradient flow. Suppose that at some time t_0 the network classifies all samples correctly. Then gradient flow converges in direction to a KKT point of the maximum-margin problem:

$$\min_{\theta} \ \tfrac{1}{2}\|\theta\|^2 \quad \text{s.t.} \quad \forall i \in [n] \ y_i \, \Phi(\theta; x_i) \geq 1.$$

The associated KKT conditions are:

$$\theta \ - \ \sum_{i=1}^{n} \lambda_i \, \nabla_\theta \big[y_i \, \Phi(\theta; x_i) \big] = 0 \qquad \text{(stationarity)} \tag{4}$$

$$y_i \, \Phi(\theta; x_i) \geq 1 \qquad \text{(primal feasibility)} \tag{5}$$

$$\lambda_i \geq 0 \qquad \text{(dual feasibility)} \tag{6}$$

$$\lambda_i = 0 \quad \text{if } y_i \, \Phi(\theta; x_i) \neq 1 \qquad \text{(complementary slackness).} \tag{7}$$

Bias with weight decay: Previous works (Haim et al., 2022; Buzaglo et al., 2023) have further analyzed the effect of explicit weight decay in this context. For simplicity, and following Buzaglo et al. (2023), we present the analysis in the binary classification case, though the argument can be extended to the multiclass setting.

Let $\ell(\Phi(x_i; \theta), y_i)$ be a loss function that takes as input the scalar prediction of the model $\Phi(\cdot; \theta)$ on sample x_i, and its corresponding label y_i. The total regularized loss is

$$L(\theta) = \sum_{i=1}^{n} \ell(\Phi(x_i; \theta), y_i) \ + \ \lambda_{\text{WD}} \, \tfrac{1}{2}\|\theta\|^2.$$

Assuming convergence ($\nabla_\theta L = 0$), the parameters satisfy

$$\theta = \sum_{i=1}^{n} \ell_i' \, \nabla_\theta \Phi(x_i; \theta), \qquad \ell_i' = -\frac{1}{\lambda_{\text{WD}}} \frac{\partial \, \ell(\Phi(x_i; \theta), y_i)}{\partial \Phi(x_i; \theta)}. \tag{8}$$

This relation shows that the trained weights again lie in the span of per-sample gradients, with coefficients $\{\ell_i'\}$ determined by the derivative of the loss. Importantly, equation 8 is structurally equivalent to the stationarity condition in the KKT system of the max-margin problem: in both formulations, the parameters are expressed as a linear combination of margin-gradient directions. Furthermore, if ℓ is the logistic loss function, then the coefficients $\{\ell_i'\}$ of this linear combination are non-negative.

E   LIMITATIONS OF AVERAGE-CASE METRICS

A common evaluation practice in the membership inference literature is to report average-case metrics such as balanced accuracy or ROC-AUC. While convenient, these metrics are misaligned with the privacy risks that matter in practice.

First, average-case metrics obscure worst-case behavior. Balanced accuracy treats false positives and false negatives symmetrically, yet in privacy attacks the costs are asymmetric: false positives (incorrectly labeling non-members as members) undermine reliability, whereas false negatives are typically less harmful. Second, aggregate metrics such as AUC average performance across the entire ROC curve, including regions of high false-positive rates that are irrelevant in practice. As emphasized by Carlini et al. (2022), an attack may achieve high AUC while completely failing to recover any members at $\leq 0.1\%$ FPR. Conversely, an attack that reliably recovers only a small subset of members may achieve modest AUC but still constitute a severe privacy breach. For this reason, recent work on membership inference (Carlini et al., 2022; Zarifzadeh et al., 2023) has adopted TPR at low FPR as the primary evaluation metric.

This mismatch is evident in our results. Table 1 reports performance of several attacks in the "no auxiliary knowledge" setting. On CIFAR-10, both our attack and the GradNorm baseline achieve AUC ≈ 0.81. However, this similarity is misleading: GradNorm leverages model confidence, and its apparent effectiveness comes from the fact that non-members in this scenario has low confidence. By contrast, as shown by Haim et al. (2022), the truly memorized samples are those near the decision boundary. Our attack explicitly targets such near-margin points, yielding much higher TPR at very low FPR (e.g., 2.76% vs. 0.11% at 0.01% FPR). This gap illustrates why average-case metrics like AUC are problematic: they make GradNorm appear competitive, while in reality it fails where privacy evaluation matters most—the ultra–low-FPR regime

F   REBUTTAL ADDITIONAL RESULTS

All new results are presented here for convenient of the reviewers and are already integrated into the main paper and appendix.
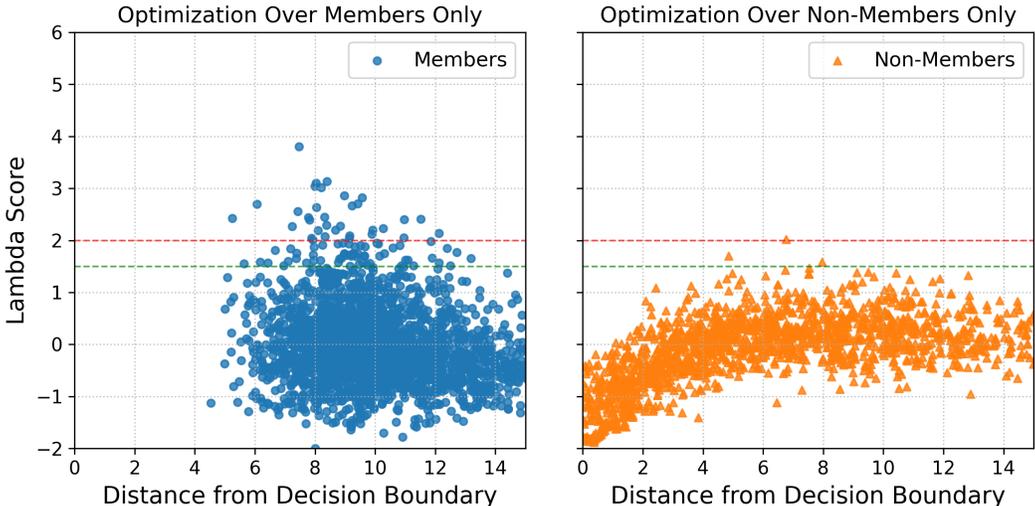
F.1   VISUAL RESULTS

Figure S4: ***Behavior when the superset contains only members or only non-members.*** *We plot the learned λ scores when the coefficients are optimized on (i) a superset containing only non-members (which can be a reference non-member set), and (ii) a superset containing only members. Even though these optimizations are performed separately, many member samples still receive higher λ scores than non members.*

F.2   QUANTITATIVE RESULTS

Attack	VGG16			ResNet50		
	AUC	@0.01 %	@0.0 %	AUC	@0.01 %	@0.0 %
LiRA	0.75	0.62	0.18	0.79	1.02	0.26
RMIA	**0.78**	0.69	0.06	0.78	0.09	0.02
Ours	**0.78**	**1.59**	**0.56**	**0.82**	**1.80**	**0.78**

Table T15: ***Membership Inference Results on Different Architectures.*** *Performance of LiRA, RMIA, and our method on VGG16 and ResNet50. We report AUC and TPR at fixed false-positive rates (FPR = 0.01% and 0.0%).*

Attack	AUC	@0.1 %	@0.0 %
Attack-P	0.76	0.38	0.06
Attack-R	0.74	1.73	0.32
LiRA	**0.80**	2.98	**1.20**
RMIA	**0.80**	2.43	0.14
Ours	0.75	**3.01**	0.94

Table T16: ***Comparison under limited coverage (10%).*** *We compare our method with previous attacks when the candidate superset covers only 10% of the training data in our realistic no auxiliary knowledge setting. Even under this low coverage, our results are comparable to the best competitors.*

Attack	AUC	@0.01 %	@0.00 %
Attack-R	0.75	0.01	0.00
Attack-P	0.76	0.12	0.00
LiRA	**0.80**	0.54	0.11
Ours	0.79	**3.00**	**0.54**

Table T17: ***Membership inference with a 250K candidate pool (CIFAR-10).*** *We compare ImpMIA to other MIA baselines under the realistic no auxiliary knowledge setting. We report AUC and TPR at fixed false-positive rates (FPR = 0.01% and 0.00%).*

Variant	AUC	@0.01 %	@0.0 %
Trimmed mean only	0.74	2.58	1.18
Robust SNR only	**0.85**	2.51	0.89
Fusion (trimmed mean + SNR)	0.82	2.60	1.23
+ Boost1 (class-level margins)	0.82	2.59	1.23
+ Boost2 (sample-level margins)	0.81	2.69	1.39
+ Trim division	0.82	**2.84**	1.31
ImpMIA	0.81	2.76	**1.41**

Table T18: ***Ablation of ImpMIA Components (no auxiliary knowledge setting) for CIFAR-10.*** *Performance of different scoring variants and incremental boosts. We report AUC and TPR at fixed false-positive rates (FPR = 0.01% and 0.0%).*